

Learning Position From Vehicle Vibration Using an Inertial Measurement Unit

Barak Or, *Member, IEEE*, Nimrod Segol, Areej Eweida, and, Maxim Freydin, *Member, IEEE*

Abstract—This paper presents a novel approach to vehicle positioning that operates without reliance on the global navigation satellite system (GNSS). Traditional GNSS approaches are vulnerable to interference in certain environments, rendering them unreliable in situations such as urban canyons, under flyovers, or in low reception areas. This study proposes a vehicle positioning method based on learning the road signature from accelerometer and gyroscope measurements obtained by an inertial measurement unit (IMU) sensor. In our approach, the route is divided into segments, each with a distinct signature that the IMU can detect through the vibrations of a vehicle in response to subtle changes in the road surface. The study presents two different data-driven methods for learning the road segment from IMU measurements. One method is based on convolutional neural networks and the other on ensemble random forest applied to handcrafted features. Additionally, the authors present an algorithm to deduce the position of a vehicle in real-time using the learned road segment. The approach was applied in two positioning tasks: (i) a car along a 6 [km] route in a dense urban area; (ii) an e-scooter on a 1 [km] route that combined road and pavement surfaces. The mean error between the proposed method’s position and the ground truth was approximately 50 [m] for the car and 30 [m] for the e-scooter. Compared to a solution based on time integration of the IMU measurements, the proposed approach has a mean error of more than 5 times better for e-scooters and 20 times better for cars.

Index Terms—Deep Neural Network, Inertial Measurement Unit, Inertial Navigation System, Machine Learning, Supervised Learning.

I. INTRODUCTION

IN various domains and applications, continuous real-time positioning solutions are required. Currently, outdoor positioning technology relies heavily on satellite navigation devices such as GNSS receivers. This includes GPS, GLONASS, Galileo, Beidou, and other satellite navigation systems [1]–[3]. Drivers commonly rely on GNSS technology for positioning and navigation, often using their smartphones for this purpose [2], [4]. However, GNSS requires a line of sight with multiple satellites and is thus unsuitable for indoor positioning applications including navigating through tunnels and indoor parking lots [5]–[8]. Additionally, there are scenarios in which GNSS does not offer sufficient accuracy for certain outdoor positioning applications [9]–[11].

Given the limitation of GNSS, there are approaches that make use of other sensors to compensate. In many scenarios, GNSS measurements are fused with maps and additional sensors to ensure continuous localization and improve accuracy.

A key example is autonomous vehicles (AVs) [12], [13] where there exists a need for continuous availability beyond that provided by GNSS. It is therefore common to perform fusion with additional sensors such as cameras, LiDARs, inertial sensors, odometry, and others [14]–[16]. Unfortunately, these sensors are usually expensive, and the quality of the data they provide depends on various physical conditions, such as lighting and the presence of occlusions. Hence, there are no accurate and continuous positioning solutions for vehicles that operate both indoors and outdoors. This work presents an approach that relies only on a single IMU sensor and is a step towards a continuous solution for a broad range of scenarios and environments.

The positioning approach suggested here applies machine learning to inertial sensor readings. Inertial sensors are commonplace in mobile devices and have a broad range of applications including in mobility and transportation. Indeed, various authors have utilized the IMU sensors for many tasks including identifying driver activity, detecting car accidents, and other [17]–[19]. In the navigation domain, it is common to fuse inertial with GNSS measurements in an INS/GNSS (inertial navigation system) fusion scheme. The IMU typically consists of two sensors: an accelerometer that measures specific force and a gyroscope that measures angular velocity. Positioning is deduced by integrating (with respect to time) both the accelerometer and gyroscope measurements and fusing the high-rate low-accuracy integrated solution with a low-rate high-accuracy GNSS measurement. This approach is sometimes referred to as strap-down inertial navigation (SINS) where it could be said that dead reckoning is performed between each pair of GNSS measurements. The SINS approach is vulnerable to drift, leading rapidly to large errors in the solution [3]. While this work uses the common and affordable IMU sensor which has the significant advantage of high availability, we do not use dead reckoning. Instead, we use the power of machine learning (ML) and deep learning (DL). Machine learning methods presented impressive results in a wide range of domains in recent years [20], [21]. Therefore, the authors of this work propose to utilize them to derive a positioning method from an IMU sensor that does not suffer from rapidly increasing drift.

In previous related work, DL-based models were integrated into a wide range of navigation and positioning tasks. In [22] neural networks were trained to regress linear velocities from inertial sensors and use these predictions to constrain accelerometer readings. In [23], a DL-based model was developed to address the limitations of wheel odometry in land vehicle navigation. In [24], researchers used long short-term

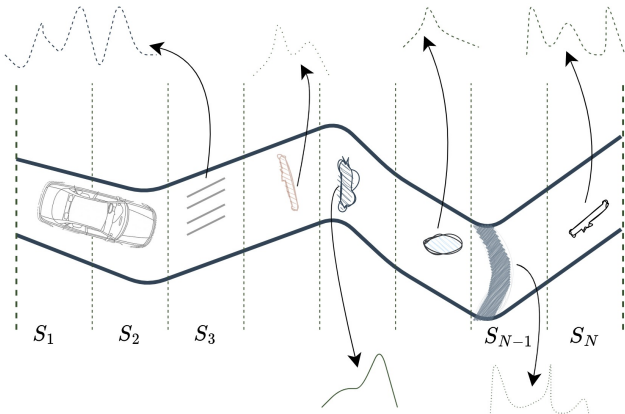


Fig. 1: An illustration of road segmentation. The proposed methodology is applied for ground vehicle positioning tasks as illustrated. The route is broken into N segments where the IMU measurements are classified into one of the N segments S_i , based on unique time-series signal signatures. In this illustration, there is a different road texture in each segment, producing a different and unique IMU signal.

memory (LSTM) networks to learn the road curvature and other features in order to estimate the process noise covariance in a linear Kalman filter. In [25], an approach to address GNSS outages was proposed involving a DL-based multi-model approach and an extended Kalman filter. [26], presents a DL-based model that utilized a stream of measurements from a low-cost IMU to estimate the speed of a car driving in an urban area. In [27], a data-driven approach using a DL-based model is presented to learn the yaw mounting angle of a smartphone equipped with an IMU and strapped to a car. In [28] the authors propose the use of a neural network on WiFi signals for indoor navigation. Previously in [29] the authors introduced a new method to detect road landmarks such as bumps using a machine learning method on IMU sensor readings. This work significantly extends that past work by deriving a positioning solution.

This study presents a novel approach to vehicle positioning using only IMU measurements, without the need for GNSS or any other sensor. A machine learning model learns the road segment based on vibration measured by the IMU as illustrated in Figure 1. This work investigated two different data-driven methods to learn the road segment. The proposed methods were rigorously validated and compared to classical dead reckoning, showing significant improvements in position accuracy for a car along a 6 [km] urban route and an e-scooter on a 1 [km] mixed surface route. These findings have important implications for the development of effective and efficient vehicle positioning techniques, particularly in challenging scenarios where traditional approaches may not be feasible. To summarize,

- 1) We propose a positioning method on a given route based only on IMU measurements.
- 2) The method is data-driven and we investigated two distinct machine learning approaches that learn from the IMU readings

- 3) We collected two data sets, cars, and e-scooters, and validated our approach on these data sets.
- 4) We compared our results on these data sets with classical dead reckoning (where accelerometer and gyroscope data is rotated to an inertial frame and integrated with respect to time) and received favorable results.

The rest of the paper is organized as follows: Section II describes the data-driven approach to vehicle positioning; In particular, we elaborate on the data processing and data-driven ML and DL algorithms we employ. In Section III, a description of the real-life datasets we collected is provided, followed by the experimental results and discussion. Finally, Section IV presents concludes the work.

II. DATA DRIVEN BASED POSITIONING INFERENCE

The core concept involves utilizing an ML algorithm to determine a vehicle's current position on a given route. Specifically, a route is divided into N segments of uniform length and an ML model is trained on IMU data from the vehicle's accelerometer and gyroscope sensors to infer its current road segment. This technique, where the current road segment is inferred, is referred to as *road segmentation*, and the ML model used for this purpose is called a *road segmentor*. The midpoint of the inferred segment is then reported as the vehicle's position. Refer to Figures 1 and 2 for an illustration of this methodology and the data flowchart, respectively.

Section II-A provides a detailed description of the positioning algorithm, with Subsections II-B, II-C, and II-D elaborating on the critical components of tuning the number of road segments, processing the data, and designing the ML algorithm, respectively.

A. Algorithm Description

In this part, a detailed description of the methodology is presented. Initially, input raw measurements from the IMU are obtained, which include acceleration in units of m/s^2 and angular velocity in units of rad/s across three axes. These measurements are then passed through a processor that is thoroughly described in Subsection II-C. Our data processing approach involves taking 2 [s] of IMU measurements at a time. Specifically, if the original IMU data is sampled at a frequency of f Hz, then our initial data measurement is represented as $I_t \in \mathbb{R}^{2f \times 6}$ where t represents the time in seconds. The pre-processing stage is denoted by P and is described in detail in the following subsection.

$$P : \mathbb{R}^{2f \times 6} \rightarrow \mathbb{R}^{40 \times 6}; \quad \bar{I}_t = P(I_t). \quad (1)$$

As part of the pre-processing, we downsample the data to 20 Hz, resulting in $\bar{I}_t \in \mathbb{R}^{40 \times 6}$. Next, the processed IMU data is passed through a road segmentor, denoted by R , to infer the current road segment.

$$R : \mathbb{R}^{40 \times 6} \rightarrow [N]; \quad \tilde{S}_t = R(\bar{I}_t) \quad (2)$$

where N is the number of road segments and $\tilde{S}_t = R(\bar{I}_t)$ is the vehicle's current road segment.

This study explores two different road segmentors to infer the current road segment from processed IMU data. The first

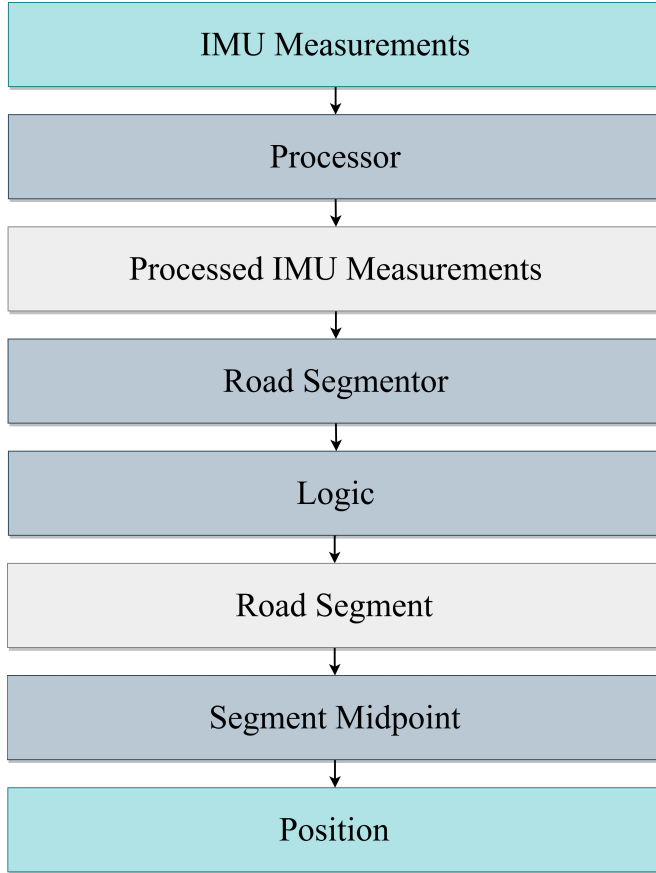


Fig. 2: Block diagram of the positioning algorithm.

road segmentor is based on a convolutional neural network (CNN) [30], while the second one employs hand-crafted features (HCF) and an ensemble random forest (Ensemble) [31]. Further details can be found in Subsection II-D.

The current segment is inferred based on the last segment (which was inferred in the previous time window of two seconds) and the output of the road segmentor. The classifier output is limited to either the current or next segment since the vehicle can only move to the next segment or remain in the current one. Denote this logic by L we have,

$$L : [N] \times [N] \rightarrow [N]; \quad S_t = L(\tilde{S}_t, S_{t-2}) \quad (3)$$

Finally, we report the position by taking the midpoints of the inferred segment. That is

$$M : [N] \rightarrow \mathbb{R}^2; \quad (x_t, y_t) = M(S_t) \quad (4)$$

where M is the midpoint of the segment S_t . Based on the described process, a positioning function is provided by

$$\Phi : \mathbb{R}^{2f \times 6} \times [N] \rightarrow \mathbb{R}^2; \quad \Phi(I_t, S_{t-2}) = M \circ L \circ R \circ P \quad (5)$$

which takes a raw IMU measurement and the previous inferred segment and outputs a position. The full algorithm is described in a block diagram in Figure 2 and in Algorithm 1.

B. Tuning the Number of Segments

The road segmentor takes a processed IMU measurement and outputs a segment number where each of the segments

Algorithm 1 Positioning from IMU measurements and a predetermined list of segment midpoints

```

1:  $S_{-2} \leftarrow 1$ 
2: for  $t = 0[s], 2[s] \dots \text{do}$ 
3:    $I_t \leftarrow \text{raw IMU}$             $\triangleright$  Read data from the sensor
4:    $\tilde{I}_t \leftarrow P(I_t)$           $\triangleright$  As described in Subsection II-C
5:    $\tilde{S}_t \leftarrow R(\tilde{I}_t)$         $\triangleright$  Road segmentors in Subsection II-D
6:   if  $\tilde{S}_t - S_{t-2} \notin [0, 1]$  then
7:      $S_t \leftarrow S_{t-2}$ 
8:   else
9:      $S_t \leftarrow \tilde{S}_t$ 
10:  end if
11:   $(x_t, y_t) \leftarrow M(S_t)$         $\triangleright$  Report the position as the
    midpoint of the inferred segment
12: end for
  
```

has the same length. Determining the best number of segments in the route is a crucial step in the positioning solution. As the number of segments increases, the road segmentation task becomes more challenging due to the increasing number of features and variations to be captured for each segment. For a given dataset with a limited number of recordings, this also means that there are more segments to distinguish between and fewer samples for each segment to learn from. On the other hand, when the route is divided into smaller segments there is the benefit of increasing the accuracy of distance estimates within each segment. This is because the midpoint of a shorter segment provides a more precise estimate of the vehicle's position within that segment.

This paper investigates the performance of a positioning solution on two datasets, each with its unique characteristics. We use a data-driven approach to determine the optimal number of road segments for each dataset using a validation set. Figures 6 and 7 present the effect of a number of segments on the average positioning error. We show that the positioning error increases when the number of road segments is either too large or too small. This highlights the importance of choosing an appropriate segment length that is tailored to the specific characteristics of the dataset and the requirements of the application.

C. Data Processing

To prepare the raw IMU data for use by the ML road segmentor, we first apply a series of processing steps to enhance the quality of the data and reduce noise. The raw data used in this study consists of measurements of acceleration in m/s^2 and angular velocity in rad/s in three axes. The preprocessor P is applied to raw data as described by Eq. (1). It is composed of,

- 1) Low-pass filter (LPF) with a cut-off frequency of 10 Hz. Most IMUs operate at sampling rates at or above 100 Hz which is significantly greater than the dynamics bandwidth of a typical vehicle [32]. This step reduces the noise inherent to low-cost inertial sensors while maintaining key signal information.
- 2) Down-sample the data to 20 Hz. To facilitate the use of our ML road segmentor with different mobile phones

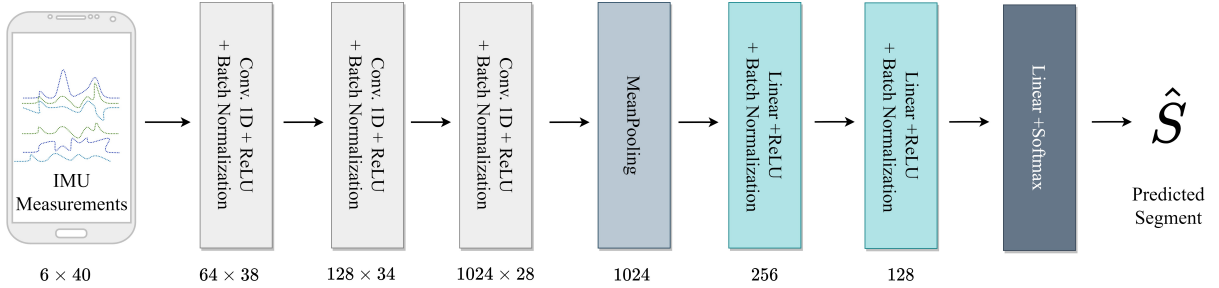


Fig. 3: The network architecture used for the CNN classifier.

that sample IMU data at different frequencies, we down-sample the data to a common frequency of 20 Hz. This step is critical for ensuring that our approach is widely applicable and can be used with different types of mobile devices and sensors.

3) Rotate the measured acceleration and angular velocity vectors to a frame where the third vector component is aligned parallel to the gravity vector (i.e., compensate for the roll and pitch angles [3]). The gravity component is then subtracted from the third component of the acceleration vector. This step makes the data more uniform and independent of the mobile device's roll and pitch installation angles.

The preprocessing steps outlined above are applied both offline during training of the ML model and online in real-time scenarios. The purpose of these steps is to simplify the raw sensor data by removing noise and other extraneous information that is not relevant to the task of road segmentation and vehicle positioning. It is noted that the above processing procedure has appeared in various prior works e.g. [3], [26], [27]. It is provided for this work to be self-contained.

D. Road Segmentors

In this section, we provide a detailed description of the machine learning methods we employed for road segmentation. Specifically, we introduce the road segmentor R , as outlined in Equation (2). The road segmentor is a critical component of our approach to vehicle positioning and can be one of two different machine learning methods. We investigate two common data-driven methods to learn position from vibrations,

1) *Convolutional neural network*: The first road segmentor we used is a CNN composed of the following layers:

- **Linear layer**: A linear transformation is applied to the data from the preceding layer.
- **Conv1D layer**: A convolutional, one-dimensional layer creates a convolution kernel that is convolved with the layer input over a single dimension to produce a vector of outputs. The dimensions of the convolutions layers are 64, 128, and 1024 with kernel sizes 3, 5 and 7.
- **Mean pooling**: Pooling layers help with better generalization capability as they perform a down-sampling feature map.
- **ReLU**: A nonlinear activation function defined by $\text{ReLU}(\alpha) = \max(\alpha, 0)$.

- **Batch normalization**: Batch normalization reduces covariate shift. The batch normalization was added after every Conv1D layer (together with the ReLU layer).

See Figure 3 for a schematic of the network. The CNN was trained for a total of 200 epochs using the cross-entropy loss function, which is commonly used in classification tasks. Specifically, we define the output of the CNN as $\tilde{y}(I, \mathbf{W})$, where \mathbf{W} represents the weights of the CNN, and I is the preprocessed IMU input. The cross-entropy loss function is then defined as:

$$\ell = - \sum_{c=1}^M y_c \log (\tilde{y}(I, \mathbf{W})) \quad (6)$$

where $y_c = 1$ if the true label y is equal to c and 0 otherwise. We used the ADAM optimizer [33] with an initial learning rate of 0.001 and multiplicative learning rate decay of 0.1 every 50 epochs. We trained the model using a Tesla V100 Nvidia GPU and took about 24 minutes per epoch.

2) *Ensemble random forest*: We evaluated a second approach for road segmentation, the ensemble random forest method. This method takes as input 702 hand-crafted features extracted from the pre-processed IMU measurements. The feature extraction process is detailed in appendix IV. We fed the features into a random forest classifier with 100 decision trees. During training, no maximum depth was specified, and all nodes were expanded until all leaves were pure. For the car's data set, the resulting decision tree estimators had an average depth of 29.19, a minimum depth of 25, and a maximum depth of 38. For the e-scooter's data set, the resulting decision tree estimators had an average depth of 37.87, a minimum depth of 31, and a maximum depth of 48.

III. EXPERIMENTS

We evaluated our positioning solution in two distinct scenarios: a car driving in a dense urban area and an e-scooter traveling on a route that includes both roads and sidewalks. As we detail in the sequel, the suggested data-driven methods significantly outperform traditional dead reckoning. In Subsection III-A we detail the data collected for both experiments, while the results of our approach are presented in Subsection III-B.

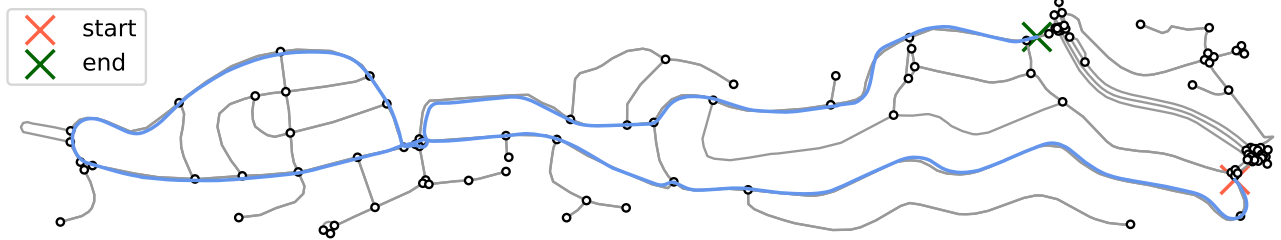


Fig. 4: The car route (blue) is shown on top of the road map (grey), taken from OpenStreetMap [34].

A. Data Collection

We collected real-world data to construct two datasets suitable for testing and validating the proposed data-driven algorithm.

1) *Cars*: We assembled a dataset consisting of 49 drives of a particular route, spanning a distance of 5919 [m], as seen in Figure 4. The data was recorded using the PhyPhox app [35] on a Galaxy A21s smartphone at a sampling rate of 200 Hz. In addition to the IMU data, GPS coordinates were also collected at a sampling rate of 1 Hz using the same app. The drives were taken in ten different cars, with five drives recorded from 9 of the cars and 4 drives from the 10th car. Two drives from each car were reserved for validation and testing. Therefore, a total of 29 drives were used for training, 10 for validation, and 10 for testing.

2) *E-scooters*: We collected a data set of 63 e-scooter drives covering a distance of 917 [m] on a predetermined route depicted in Figure 5. The drives were collected by two different drivers using different phones. The drivers were not told on which part of the route to drive on the sidewalk and on which on the road and each driver chose independently. The recordings contain IMU measurements at a frequency of 420 Hz and GPS coordinates at a frequency of 1 Hz recorded using the PhyPhox app on either a Galaxy S22 (for the first driver) or Oneplus nord2 (for the second driver) device. We employed 47 of the drives for training (24 from the first driver and 23 from the second), 8 for validation (4 from each driver), and 8 for testing (4 from each driver).

B. Experimental Results

This section presents the results of our experiments on cars and e-scooters, specifically evaluating the performance of both data-driven road segmentors described in Section II-D.

Our evaluation includes eight different measures, namely,

- **acc raw** – the raw accuracy of the classifier, i.e., using the road segmentor output.
- **acc** – the accuracy of the classifier after applying the logic described in Algorithm 1.
- **2-acc raw** – the 2 accuracy of the raw classifier, which is the percentage of segments at most 1 segment removed from the ground truth.
- **2-acc** – the 2 accuracy after applying the logic in Algorithm 1.
- **max dist raw** – the maximal distance between the midpoint of the segment reported by the raw classifier and the ground truth.

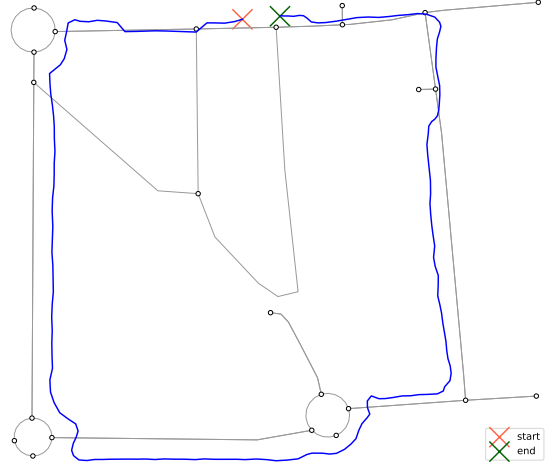


Fig. 5: The e-scooter route (blue) is shown on top of the road (grey), taken from OpenStreetMap. The route includes on and off-road segments, making for a diverse and challenging route.

- **max dist** – the maximal distance between the position reported by Algorithm 1 and the ground truth.
- **mean dist raw** – the average distance between the midpoint of the segment reported by the raw classifier and the ground truth.
- **mean dist** – the average distance between the position reported by Algorithm 1 and the ground truth.

The results of the evaluation are summarized in Table I for cars and Table II for e-scooters. All results were compared with classical dead reckoning where the IMU signals were rotated to the inertial frame and integrated with respect to time to yield location estimates.

1) *Learning car position*: To determine the optimal number of road segments for Algorithm 1, we evaluated 13 different numbers of road segments, ranging from 10 to 70 in increments of 5, as described in Subsection II-B. The optimal number of road segments was chosen based on the best performance on the validation set. Figure 6 shows the resulting average error between the output of Algorithm 1 and the GPS as a function of the number of segments for both the CNN and Ensemble road segmentors. We found that dividing the route into 40 segments yielded the lowest error on the validation set for both road segmentors.

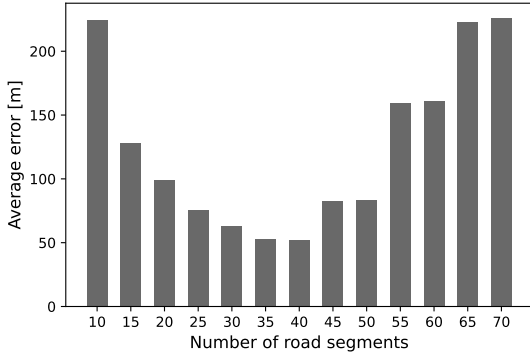
2) *Learning e-scooter position*: Learning road segments from the road vibration generated by an e-scooter is more challenging than those generated by a car. This is due to the greater freedom an e-scooter driver has in choosing a route,

Classifier	acc raw	acc	2-acc raw	2-acc	max dist raw [m]	max dist [m]	mean dist raw [m]	mean dist [m]
CNN	0.79	0.87	0.89	1	2377	296	184	53
Ensemble	0.7	0.83	0.81	1	2377	211	198	55
Dead reckoning	N.A.	N.A.	N.A.	N.A.	N.A.	2484	N.A.	1247

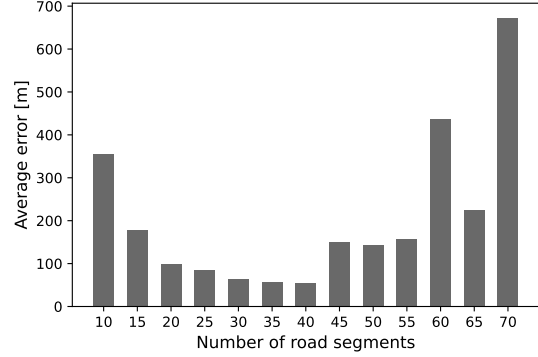
TABLE I: Results of our data-driven approaches on the cars data-set. The performance metrics are explained in Section III-B.

Classifier	acc raw	acc	2-acc raw	2-acc	max dist raw [m]	max dist [m]	mean dist raw [m]	mean dist [m]
CNN	0.58	0.72	0.70	0.96	297	149	74	32
Ensemble	0.48	0.63	0.63	0.9	316	309	97	56
Dead reckoning	N.A.	N.A.	N.A.	N.A.	N.A.	752	N.A.	316

TABLE II: Results on the e-scooters data-set.

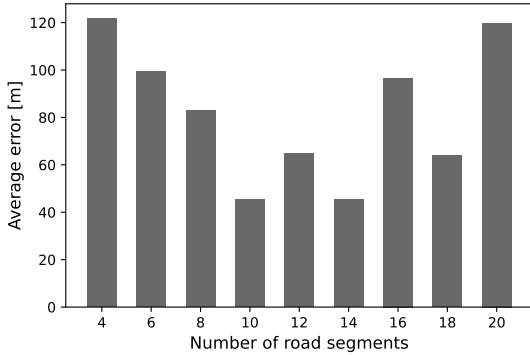


(a)

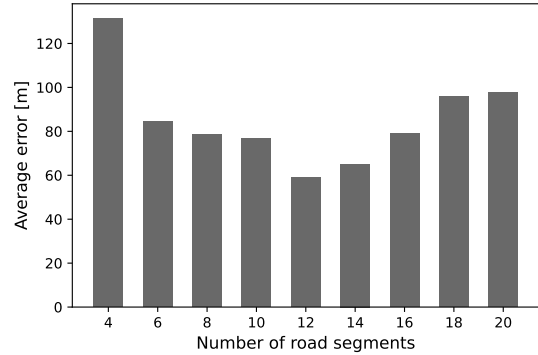


(b)

Fig. 6: Average distance error [m] vs. the number of road segments, evaluated on the validation set for cars. The results are shown for both a CNN classifier (on the left) and a classifier based on hand-crafted features and a random forest (on the right).



(a)



(b)

Fig. 7: Average distance error [m] vs. the number of road segments, evaluated on the validation set for e-scooters. The results are shown for both a CNN classifier (on the left) and a classifier based on hand-crafted features and a random forest (on the right).

resulting in a more varied road vibration signature. While a car completely fills a car lane, an e-scooter may drive on various paths on a sidewalk or road or a bicycle lane. Note the trajectory in our experiment in Figure 5 where the e-scooter drives both off and on the road. In addition, an e-scooter will be more sensitive to turns, starts, and stops, resulting in noisier IMU measurements. As a result, the road vibration signature of an e-scooter is much more varied. Despite the challenges inherent in learning road segments from the road vibrations

generated by an e-scooter, our proposed approach achieved an average error of approximately 30 [m] for a 917 [m] route. In contrast, a traditional dead reckoning approach resulted in an average error exceeding 300 [m]. Comprehensive results of our positioning solution for the e-scooter dataset are provided in Table II.

We consider 9 possibilities for the number of segments between 4 and 20 with increments of 2. For each, we partition the route into equal segments, train a road segmentor on the

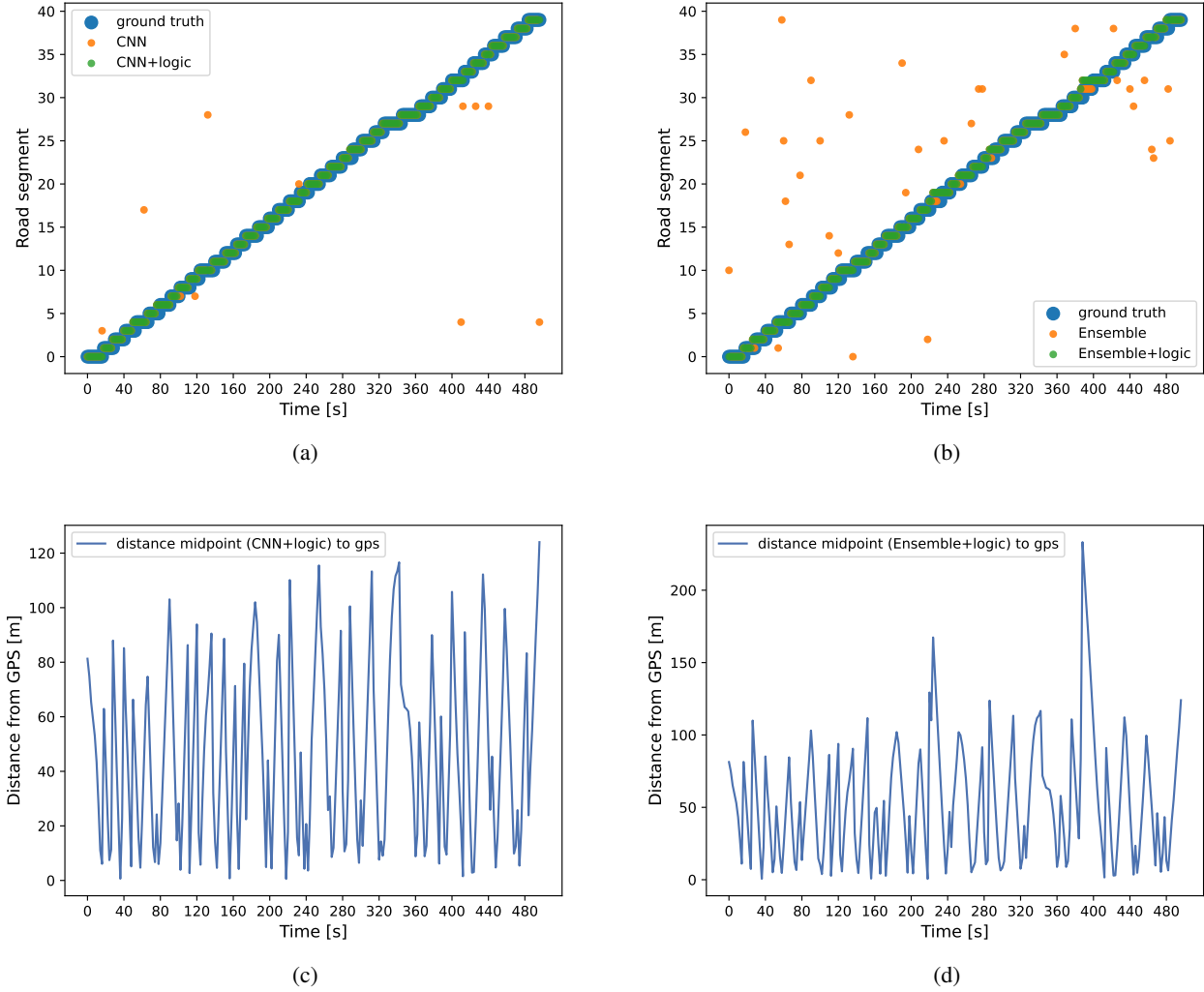


Fig. 8: Results vs. time on a particular drive from the cars test set. The top row shows the classification results obtained by the DL-based road segmentor (CNN) and the road segmentor based on the ensemble of hand-crafted features and random forest (Ensemble). Both raw and corrected classification results are presented. The bottom row shows the error between the reported position and the GPS ground truth.

training set, and test the accuracy on the validation set using Algorithm 1. In Figure 7, the average error on the validation set is plotted as a function of the number of segments for both a deep classifier and a road segmentor based on random forest and HCFs. The optimal number of segments was found to be 14 for the CNN road segmentor, and 12 for the Ensemble road segmentor based on the lowest validation error.

C. Performance Analysis

To gain insight into the effectiveness of our approach, we can compare the maximum and average errors presented in Tables I and II to those achievable with a perfect road segmentor and a vehicle traveling at a constant velocity. If a route of length L is partitioned into N segments, a perfect road segmentor would have a maximum error of $\frac{L}{2N}$. Assuming constant speed, a perfect road segmentor would achieve an average error of $\frac{L}{4N}$. To see this, let \bar{d} be the average

distance between the vehicles position and the midpoints of the segments under the constant velocity assumption, v be the constant velocity, and $T = \frac{L}{2Nv}$ be the time it takes to travel half a segment. We will then have,

$$\bar{d} = \frac{1}{T} \int_{t=0}^T \left[\frac{L}{2N} - vt \right] dt = \frac{L}{2N} - \frac{1}{2}vT \quad (7)$$

plug in $vT = \frac{L}{2N}$ and we get $\bar{d} = \frac{L}{4N}$. Simply put, when traveling at constant velocity the average distance from the midpoint of the segment is equal to one-quarter of the segment's length.

In the car experiments, the route length was 5919 [m], divided into 40 segments. This suggests a maximal error of 73 [m] and an average error of 36 [m] with a perfect road segmentor. However, our approach resulted in a maximal error of 184 [m] and 198 [m] and an average error of 53 [m] and 55 [m] for the CNN and Ensemble road segmentors,

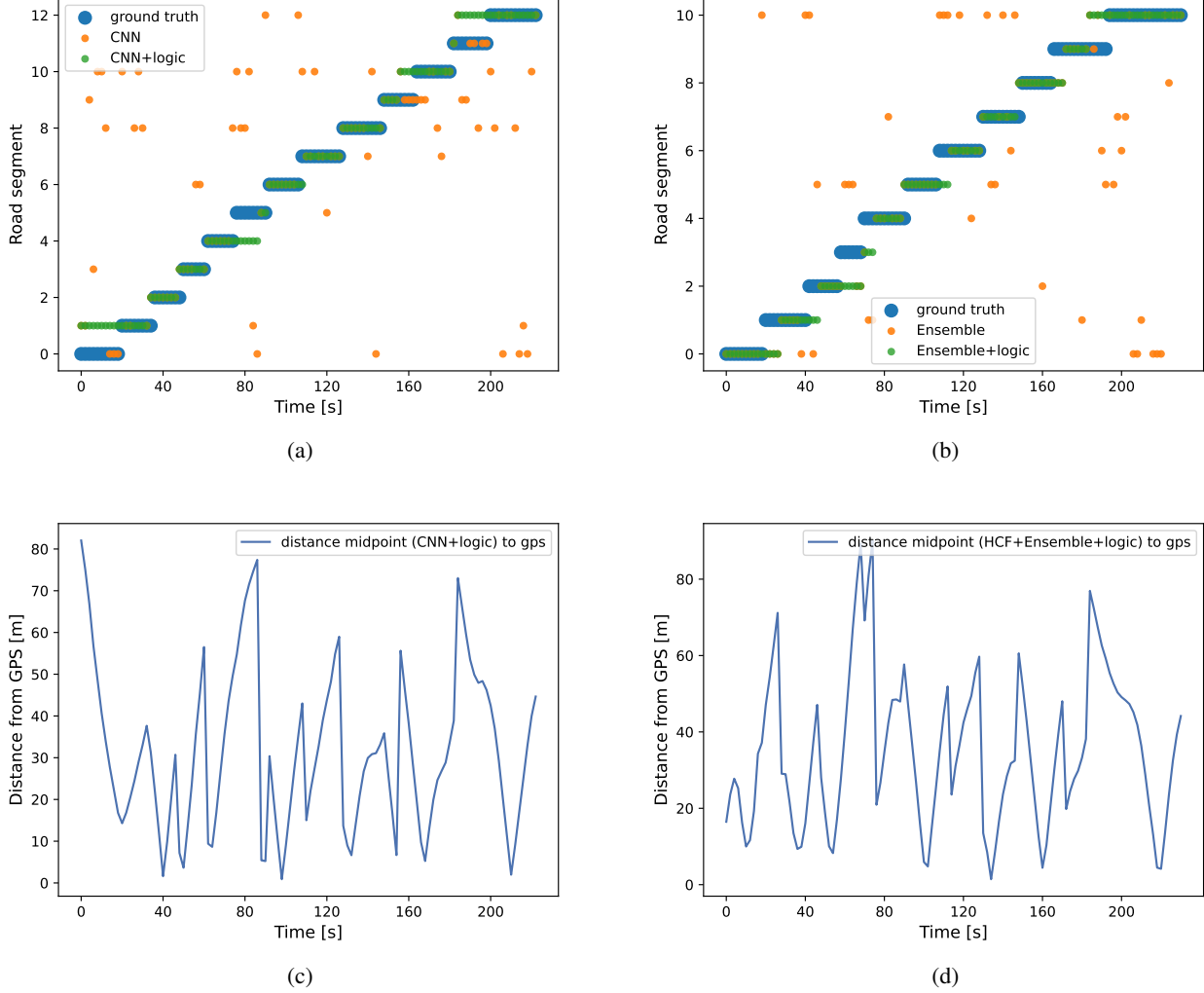


Fig. 9: Results vs. time on a particular drive from the e-scooter test set. The top row shows the classification results obtained by the DL-based road segmentor (CNN) and the road segmentor based on the ensemble of hand-crafted features and random forest (Ensemble). Both raw and corrected classification results are presented. The bottom row shows the error between the reported position and the GPS ground truth.

respectively, which are close to the ideal values. In comparison to the classical dead reckoning method, our results demonstrate that the maximal error from our road segmentors is over ten times smaller, and the average error is over twenty times smaller. Full details can be found in Table I.

In the e-scooter experiment, the route spanned 917 [m] and was divided into 14 segments for the CNN road segmentor and 12 segments for the Ensemble road segmentor. A perfect road segmentor would attain a maximal error of 32 [m] and 38 [m] for the CNN and Ensemble, respectively, with an expected average error of about 16 [m] and 19 [m] for the respective segmentors. Our experiment produced a maximal error of 149 [m] and 309 [m] for the CNN and Ensemble segmentors, respectively, with an average error of 32 [m] and 56 [m] for the CNN and Ensemble, respectively. Our results are roughly the same order of magnitude as those of the optimal road segmentor, despite the difficulty of the e-scooter localization

task. Moreover, our data-driven approaches improve the mean distance error 5 times over classical dead reckoning.

The significance of the wrapping logic function L in Eq. 3 should be noted. As shown in Tables I and II, the accuracy of both road segmentation and position estimation is significantly improved with the inclusion of the logic function L . This improvement is further evident in Figures 8 and 9, where the unprocessed road segmentation (depicted in orange) appears noisy and inaccurate. However, the accuracy is significantly enhanced upon application of the logic function L , which eliminates severe outliers. For instance, in the car dataset, the maximum distance without logic is more than ten times larger.

IV. CONCLUSIONS

This work proposes a novel approach for vehicle positioning that does not rely on the GNSS. GNSS approaches are vulnerable to interference or failure in certain environments, rendering

them unreliable in many situations. To address this issue, the proposed approach learns the road signature of a given environment and uses it for positioning via vehicle vibration, using only the IMU sensor. The approach divides a route into segments, each with a distinct signature that the IMU can detect by identifying subtle changes in the road surface. The study introduces two different methods for learning the road segment from IMU measurements, one based on convolutional neural networks and the other on ensemble random forest applied to handcrafted features. An algorithm for estimating the vehicle's road segment and deducing position in real time was presented.

The proposed approach was evaluated on a 6 [km] route in a dense urban area for a car and a 1 [km] route that combined road and pavement surfaces for an e-scooter. The mean error between the proposed method's position and the ground truth was approximately 50 [m] for the car and 30 [m] for the e-scooter, representing significant improvements over the classical dead reckoning approach. The findings demonstrate the potential for effective and efficient vehicle positioning techniques that can be used in situations where traditional GNSS approaches are unreliable.

This work opens the door to various directions for future research direction. Among them is investigating the quality of different road segmentors based on different deep learning architectures or when the road segments are not of uniform length but divided by some other criteria. It is also interesting to consider an unsupervised or semi-supervised setting where the road segment is inferred solely from the IMU reading without GPS labeling. Such a setting is relevant to indoor navigation where GPS is not available and obtaining accurate labels is difficult. Other research directions include the fusion of our approach with other sensors such as cameras or LiDAR, combining the practically unlimited availability of the IMU with the benefits of other sensors.

APPENDIX – HANDCRAFTED FEATURES FOR ENSEMBLE RANDOM FOREST

As discussed in Section II-D, one of the road segmentors considered in this work was an ensemble random forest with hand-crafted features. Here the particular features manually computed from the processed IMU signals are detailed. From the initial 6 channels, $\omega_x, \omega_y, \omega_z, a_x, a_y, a_z$ of processed IMU data we generate additional 42 channels. The numerical derivatives, $\omega_x^d, \omega_y^d, \omega_z^d, a_x^d, a_y^d, a_z^d$ the numerical integrals, $\omega_x^i, \omega_y^i, \omega_z^i, a_x^i, a_y^i, a_z^i$ the quotients, $\frac{\omega_x}{\omega_y}, \frac{\omega_y}{\omega_x}, \frac{\omega_z}{\omega_x}, \frac{\omega_x}{\omega_z}, \frac{\omega_y}{\omega_z}, \frac{\omega_z}{\omega_y}, \frac{a_x}{a_y}, \frac{a_y}{a_x}, \frac{a_z}{a_x}, \frac{a_x}{a_z}, \frac{a_y}{a_z}, \frac{a_z}{a_y}$ the quotients of the numerical integrals, $\frac{\omega_x^i}{\omega_y^i}, \frac{\omega_y^i}{\omega_x^i}, \frac{\omega_z^i}{\omega_x^i}, \frac{\omega_x^i}{\omega_z^i}, \frac{\omega_y^i}{\omega_z^i}, \frac{\omega_z^i}{\omega_y^i}, \frac{a_x^i}{a_y^i}, \frac{a_y^i}{a_x^i}, \frac{a_z^i}{a_x^i}, \frac{a_x^i}{a_z^i}, \frac{a_y^i}{a_z^i}, \frac{a_z^i}{a_y^i}$ and the amplitude of the Fourier coefficients $\mathcal{F}\{\omega_x\}, \mathcal{F}\{\omega_y\}, \mathcal{F}\{\omega_z\}, \mathcal{F}\{a_x\}, \mathcal{F}\{a_y\}, \mathcal{F}\{a_z\}$. We extracted various features from the 48 channels of our IMU measurements, except for the Fourier coefficients. The following 12 features were computed: mean, standard deviation, minimum, maximum, median, median absolute deviation, second moment, skewness, kurtosis, interquartile range, spectral entropy, and largest value divided by smallest

in absolute value. For the 24 quotient channels, we also computed the mean absolute deviation. For the 6 channels of Fourier coefficients, we computed all of the features above, with the exception of spectral entropy, resulting in additional 66 channels. We also computed the signal magnitudes area for the following triplets $\{\omega_x, \omega_y, \omega_z\}, \{a_x, a_y, a_z\}, \{a_x^d, a_y^d, a_z^d\}, \{\omega_x^d, \omega_y^d, \omega_z^d\}, \{a_x^i, a_y^i, a_z^i\}, \{\omega_x^i, \omega_y^i, \omega_z^i\}, \{\mathcal{F}\{\omega_x\}, \mathcal{F}\{\omega_y\}, \mathcal{F}\{\omega_z\}\}$ and $\{\mathcal{F}\{a_x\}, \mathcal{F}\{a_y\}, \mathcal{F}\{a_z\}\}$ for additional 8 channels. Additionally, we computed 24 correlation coefficients, between the following couples $\{\omega_x, \omega_y\}, \{\omega_x, \omega_z\}, \{\omega_x, a_z\}, \{a_x, a_y\}, \{a_x, a_z\}, \{a_y, a_z\}, \{\omega_x^d, \omega_y^d\}, \{\omega_x^d, \omega_z^d\}, \omega_x^d, \omega_z^d, \{a_x^d, a_y^d\}, \{a_x^d, a_z^d\}, \{a_y^d, a_z^d\}, \{\omega_x^i, \omega_y^i\}, \{\omega_x^i, \omega_z^i\}, \{\omega_x^i, a_z^i\}, \{a_x^i, a_y^i\}, \{a_x^i, a_z^i\}, \{a_y^i, a_z^i\}, \{\mathcal{F}\{a_x\}, \mathcal{F}\{a_y\}\}, \{\mathcal{F}\{a_y\}, \mathcal{F}\{a_z\}\}, \{\mathcal{F}\{a_x\}, \mathcal{F}\{a_z\}\}, \{\mathcal{F}\{\omega_x\}, \mathcal{F}\{\omega_y\}\}, \{\mathcal{F}\{\omega_y\}, \mathcal{F}\{\omega_z\}\}, \text{ and } \{\mathcal{F}\{\omega_x\}, \mathcal{F}\{\omega_y\}\}$. Lastly, we employed an order 2 vector autoregressive model to fit the IMU measurements and appended the resulting coefficients as additional features.

REFERENCES

- [1] R. B. Langley, P. J. Teunissen, and O. Montenbruck, “Introduction to gnss,” *Springer handbook of global navigation satellite systems*, pp. 3–23, 2017.
- [2] F. Zangenehnejad and Y. Gao, “Gnss smartphones positioning: Advances, challenges, opportunities, and future perspectives,” *Satellite navigation*, vol. 2, pp. 1–23, 2021.
- [3] J. Farrell, *Aided navigation: GPS with high rate sensors*. McGraw-Hill, Inc., 2008.
- [4] J. Wahlström, I. Skog, P. Händel, and A. Nehorai, “Imu-based smartphone-to-vehicle positioning,” *IEEE Transactions on Intelligent Vehicles*, vol. 1, no. 2, pp. 139–147, 2016.
- [5] N. El-Sheimy and Y. Li, “Indoor navigation: State of the art and future trends,” *Satellite Navigation*, vol. 2, no. 1, pp. 1–23, 2021.
- [6] A. Francis, A. Faust, H.-T. L. Chiang, J. Hsu, J. C. Kew, M. Fiser, and T.-W. E. Lee, “Long-range indoor navigation with prm-rl,” *IEEE Transactions on Robotics*, vol. 36, no. 4, pp. 1115–1134, 2020.
- [7] O. Al Hammadi, A. Al Hebsi, M. J. Zemerly, and J. W. Ng, “Indoor localization and guidance using portable smartphones,” in *2012 IEEE/WIC/ACM International Conferences on Web Intelligence and Intelligent Agent Technology*, vol. 3. IEEE, 2012, pp. 337–341.
- [8] C. Zhao, A. Song, Y. Zhu, S. Jiang, F. Liao, and Y. Du, “Data-driven indoor positioning correction for infrastructure-enabled autonomous driving systems: A lifelong framework,” *IEEE Transactions on Intelligent Transportation Systems*, 2023.
- [9] N. Zhu, J. Marais, D. Bétaire, and M. Berbineau, “Gnss position integrity in urban environments: A review of literature,” *IEEE Transactions on Intelligent Transportation Systems*, vol. 19, no. 9, pp. 2762–2778, 2018.
- [10] H. Jing, Y. Gao, S. Shahbeigi, and M. Dianati, “Integrity monitoring of gnss/ins based positioning systems for autonomous vehicles: State-of-the-art and open challenges,” *IEEE Transactions on Intelligent Transportation Systems*, 2022.
- [11] C. Rizos, “Locata: A positioning system for indoor and outdoor applications where gnss does not work,” in *Proceedings of the 18th Association of Public Authority Surveyors Conference*, 2013, pp. 73–83.
- [12] D. J. Yeong, G. Velasco-Hernandez, J. Barry, and J. Walsh, “Sensor and sensor fusion technology in autonomous vehicles: A review,” *Sensors*, vol. 21, no. 6, p. 2140, 2021.
- [13] X. Meng, H. Wang, and B. Liu, “A robust vehicle localization approach based on gnss/imu/dmli/lidar sensor fusion for autonomous vehicles,” *Sensors*, vol. 17, no. 9, p. 2140, 2017.
- [14] A. Ziebinski, R. Cupek, H. Erdogan, and S. Waechter, “A survey of adas technologies for the future perspective of sensor fusion,” in *Computational Collective Intelligence: 8th International Conference, ICCCI 2016, Halkidiki, Greece, September 28-30, 2016. Proceedings, Part II 8*. Springer, 2016, pp. 135–146.
- [15] S. Campbell, N. O’Mahony, L. Krpalcova, D. Riordan, J. Walsh, A. Murphy, and C. Ryan, “Sensor technology in autonomous vehicles: A review,” in *2018 29th Irish Signals and Systems Conference (ISSC)*. IEEE, 2018, pp. 1–4.

- [16] A. Ibsch, S. Stümper, H. Altlinger, M. Neuhausen, M. Tschentscher, M. Schlipring, J. Salinen, and A. Knoll, "Towards autonomous driving in a parking garage: Vehicle localization and tracking using environment-embedded lidar sensors," in *2013 IEEE intelligent vehicles symposium (IV)*. IEEE, 2013, pp. 829–834.
- [17] J. Wahlström, I. Skog, and P. Händel, "Smartphone-based vehicle telematics: A ten-year anniversary," *IEEE Transactions on Intelligent Transportation Systems*, vol. 18, no. 10, pp. 2802–2825, 2017.
- [18] T. K. Chan, C. S. Chin, H. Chen, and X. Zhong, "A comprehensive review of driver behavior analysis utilizing smartphones," *IEEE Transactions on Intelligent Transportation Systems*, vol. 21, no. 10, pp. 4444–4475, 2019.
- [19] S. Mozaffari, O. Y. Al-Jarrah, M. Dianati, P. Jennings, and A. Mouzakis, "Deep learning-based vehicle behavior prediction for autonomous driving applications: A review," *IEEE Transactions on Intelligent Transportation Systems*, vol. 23, no. 1, pp. 33–47, 2020.
- [20] Y. LeCun, Y. Bengio, and G. Hinton, "Deep learning," *nature*, vol. 521, no. 7553, pp. 436–444, 2015.
- [21] Y. Bengio, I. Goodfellow, and A. Courville, *Deep learning*. MIT press Cambridge, MA, USA, 2017, vol. 1.
- [22] H. Yan, Q. Shan, and Y. Furukawa, "RIDI: Robust IMU double integration," in *Proceedings of the European Conference on Computer Vision (ECCV)*, 2018, pp. 621–636.
- [23] M. Brossard and S. Bonnabel, "Learning wheel odometry and imu errors for localization," in *2019 International Conference on Robotics and Automation (ICRA)*. IEEE, 2019, pp. 291–297.
- [24] B. Or and I. Klein, "Learning vehicle trajectory uncertainty," *arXiv preprint arXiv:2206.04409*, 2022.
- [25] J. Liu and G. Guo, "Vehicle localization during gps outages with extended kalman filter and deep learning," *IEEE Transactions on Instrumentation and Measurement*, vol. 70, pp. 1–10, 2021.
- [26] M. Freydin and B. Or, "Learning car speed using inertial sensors for dead reckoning navigation," *IEEE Sensors Letters*, vol. 6, no. 9, pp. 1–4, 2022.
- [27] M. Freydin, N. Sfaradi, N. Segol, A. Eweida, and B. Or, "Mountnet: Learning an inertial sensor mounting angle with deep neural networks," *arXiv preprint arXiv:2212.11120*, 2022.
- [28] W. Shao, H. Luo, F. Zhao, Y. Ma, Z. Zhao, and A. Crivello, "Indoor positioning based on fingerprint-image and deep learning," *Ieee Access*, vol. 6, pp. 74 699–74 712, 2018.
- [29] B. Or, M. Freydin, and G. Ben-haim, "System and method for estimating a location of a vehicle using inertial sensors," Jan. 3 2023, uS Patent 11,543,245.
- [30] H. Ismail Fawaz, G. Forestier, J. Weber, L. Idoumghar, and P.-A. Muller, "Deep learning for time series classification: a review," *Data mining and knowledge discovery*, vol. 33, no. 4, pp. 917–963, 2019.
- [31] C. Zhang and Y. Ma, *Ensemble machine learning: methods and applications*. Springer, 2012.
- [32] R. Rajamani, *Vehicle dynamics and control*. Springer Science & Business Media, 2011.
- [33] D. P. Kingma and J. Ba, "Adam: A method for stochastic optimization," *arXiv preprint arXiv:1412.6980*, 2014.
- [34] J. Bennett, *OpenStreetMap*. Packt Publishing Ltd, 2010.
- [35] S. Staacks, S. Hütt, H. Heinke, and C. Stampfer, "Advanced tools for smartphone-based experiments: phyphox," *Physics education*, vol. 53, no. 4, p. 045009, 2018.



Barak Or (Member, IEEE) received a B.Sc. degree in aerospace engineering (2016), a B.A. degree (cum laude) in economics and management (2016), and an M.Sc. degree in aerospace engineering (2018) from the Technion–Israel Institute of Technology. He graduated with a Ph.D. degree from the University of Haifa, Haifa (2022). He founded ALMA Technologies Ltd. (2021), focusing on Navigation and ML algorithms. His research interests include navigation, deep learning, sensor fusion, and estimation theory.



Nimrod Segol received his B.Sc. (2015, Cum Laude) and M.Sc. (2018) degrees in Mathematics from the Technion – Israel Institute of Technology. He is a senior algorithm engineer at ALMA Technologies Ltd. and his research interests include deep learning, ML, and statistics.



Areej Eweida received her B.Sc. (2022) degree in Aerospace Engineering from the Technion – Israel Institute of Technology. She is an algorithm engineer at ALMA Technologies Ltd. She is starting an M.Sc. Her research interests include estimation theory, signal processing, and deep learning.



Maxim Freydin (Member, IEEE) received his B.Sc. (2017, Summa Cum Laude) and Ph.D. (2021) degrees in Aerospace Engineering from the Technion – Israel Institute of Technology. He is the VP of R&D at ALMA Technologies Ltd. and his research interests include navigation, signal processing, deep learning, and computational fluid-structure interaction.